Effects of Fluid Flow Rate and Stress Amplitude on the Initiation and Growth Behavior of Corrosion Pits on an Annealed Carbon Steel*

Sotomi ISHIHARA**, Kazuaki SHIOZAWA**,
Kazyu MIYAO** and Masato INOUE**

In order to clarify the effects of the fluid flow rate and stress amplitude on the initiation and growth behavior of corrosion pits, round, smooth specimens were rotated at various speeds in sodium chloride aqueous solution. The results are summarized as follows: (1) The pit growth behavior was adequately predicted by Eq.(1), regardless of the fluid flow rates and stress amplitudes. (2) The pit initiation time decreases with an increase in the fluid flow rate and stress amplitudes. (3) For small pits whose sizes are about 0.03 mm, the pit growth rates increase with an increase in the fluid flow rate, while the growth rates for pits above 0.08 mm are independent of the fluid flow rate and smaller than those of 0.03 mm. The pit growth rates in the case of 100 MPa are 5~10 times larger than those of the nonstressing condition.

Key Words: Corrosion Fatigue, Corrosion Pits, Pit Initiation, Pit Growth, Carbon Steel, Fluid Flow Rate, Stress Amplitude

1. Introduction

It is well known that corrosion pits initiate and grow in the early stage of the corrosion fatigue process. Corrosion cracks start to grow from these corrosion pits and cause the final failure of the specimen. In corrosion fatigue, the fatigue limit disappears, because, even at low stress amplitude, cracks can initiate and grow from these corrosion pits.

In clarifying the damage evolution during the corrosion fatigue process, it is important to investigate the initiation and growth behavior of the corrosion pits. Many studies have investigated crack initiation and growth behavior during the corrosion fatigue process[1]~[5]; however, only a few studies have examined pit initiation and growth behavior[6],[7].

In the present study, we conducted corrosion fatigue tests in sodium chloride aqueous solution using annealed carbon steel JIS S45C, and clarified the effects of the fluid flow rate and stress amplitude on the initiation and growth behaviors of the corrosion pits.

* Received 26th November, 1991. Paper No. 91-0012 A
** Faculty of Engineering, Toyama University, 3190 Gofuku, Toyama 930, Japan

2. Specimens and Experimental Procedures

2.1 Specimens

The material tested was carbon steel JIS S45C. Its chemical composition and mechanical properties are listed in Table 1 and Table 2, respectively. The material was annealed at 1 173 K for 1 hour and machined into the figure shown in Fig. 1. After mechanical polishing with emery paper, specimens were annealed at 923 K for 1 hour, and then electropolished prior to the fatigue tests.

Table 1 Chemical compositions of the material

(wt%)

C	Mn	Si	P	S
0.46	0.81	0.23	0.022	0.018

Table 2 Mechanical properties of the specimen

Yield Strength (MPa)	Tensile Strength (MPa)	Elongation (%)
317	624	48.7

2.2 Experimental procedures

As a corrosive environment, sodium chloride aqueous solution (3% in wt %) kept at 298 K was used. It was circulated between the corrosion vessel containing the specimen and the tank by means of a pump. Air was continuously supplied to the tank by air pump so as to cause saturation of the dissolved oxygen in solution. New solution was used every day.

The flow rates of the corrosive environment were changed by rotating the specimen at various speeds. In this case, the flow rate v is given by the following expression, $v=(2\pi rf)/60$, where r is specimen radius and f is the rotating speed of the specimen. In order to investigate the pit initiation and growth behavior, the replica method was employed, and 8 selected pits were successively observed during the corrosion fatigue process for each of the experimental conditions. The number of times the replicas were sampled was determined so as to minimize the effects of the replica on the pit initiation and growth behavior. The pit diameters were measured by an optical microscope. The pit depths were determined by measuring the depths where clear focus both at the specimen surface and at the bottom of the pit was obtained.

For the loading tests, an Ono-type rotating bending fatigue machine was used.

3. Experimental Results

3.1 The pit initiation and growth behavior

In order to investigate the pit initiation and growth behavior, successive observations of the specimen surface during the corrosion fatigue process were performed. Figure 2 shows an example of the pit growth behavior obtained under the conditions of $\sigma=100$ MPa and $f=2\,000$ rpm. As seen from this figure, the pit sizes increase and their shapes change with time. Some of the pits ceased to grow after a few hours. Figure 3 shows the variations in both the pit length at the specimen surface snd the pit depth with time under the condition of $\sigma=0$ MPa. In this figure, linear relationships between the pit length $2c$ or the pit depth d_p and time exist on the log-log plots, and the following expressions are deduced:

$$2c=(2c)_0(t/t_{ic})^{A_c}$$
$$d_p=d_0(t/t_{ip})^{A_p} \qquad (1)$$

where t_{ic} and t_{ip} denote the times when the pit whose size is $2c=(2c)_0$ and $d_p=d_0$ initiates, respectively, and A_c and A_p are constants. These relationships are also confirmed by the loading tests. Many studies[6],[7], report that the pit growth law is given by Eq.(1). In the present study, it is determined that Eq.(1) is also

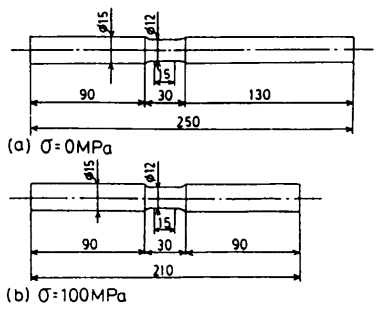

Fig. 1 Shape and dimensions of the specimen

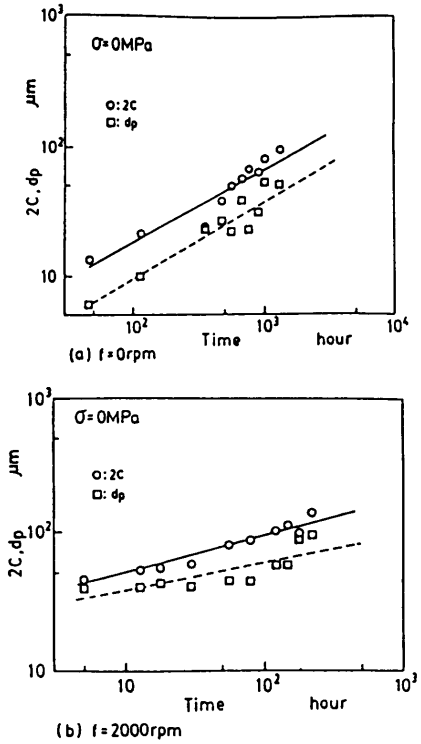

Fig. 3 Variations of pit length and pit depth with time

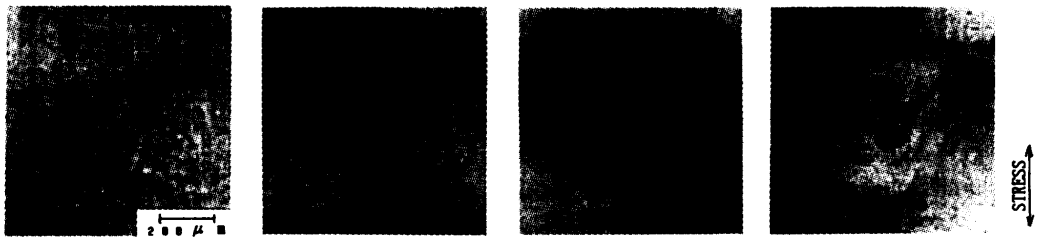

(a) 0 hour (N=0) (b) 2.0 hour ($N=2.4\times10^5$) (c) 4.0 hour ($N=4.8\times10^5$) (d) 7.0 hour ($N=8.4\times10^5$)

Fig. 2 An example of pit growth behavior ($\sigma=100$ MPa, $f=2\,000$ rpm)

applicable under conditions of variable flow rate.

3.2 Probabilistic distribution of t_i, t_p, A_i and A_p

The values of t_i, t_p, A_i and A_p can be determined by approximating the experimental data with Eq.(1). In the present case, the conditions $(2c)_0=d_0=30$ μm were adopted. Figure 4 shows the distributions of t_{ic} plotted in the Weibull probabilistic paper. Figures 4(a) and (b) correspond to the conditions of $\sigma=0$ MPa snd 100 MPa, respectively. As seen from these figures, t_{ic} decreases with an increase in the fluid flow rate. In the case of $\sigma=100$ MPa, t_{ic} is smaller than that under the condition of $\sigma=0$ MPa. These experimental results are common to those of t_{ip}. Figure 5 shows the Weibull plots of A_c for both $\sigma=0$ MPa and 100 MPa. In the case of $\sigma=0$ MPa, A_c decreases with an increase in the fluid flow rate, while in the case of $\sigma=100$ MPa, this tendency is not clearly observed. Furthermore, we can see that the values of A_c become larger with an increase in stress amplitude. The same tendency was also observed in the results of A_p.

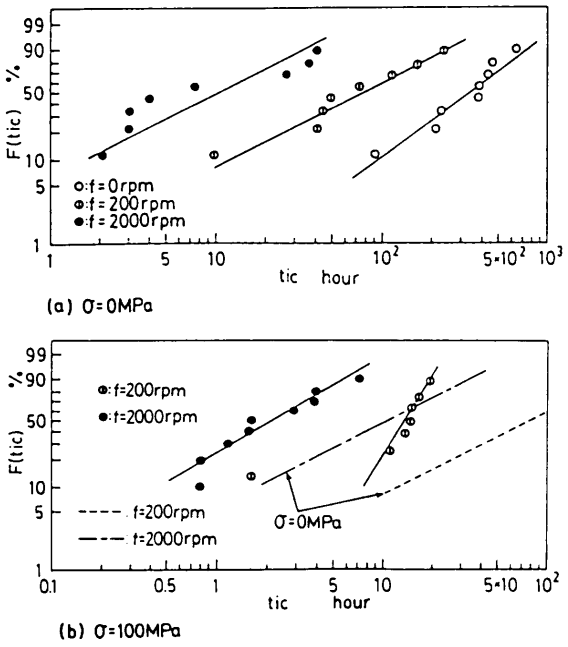

Fig. 4 Distributions of the pit initiation time plotted on the Weibull probabilistic paper

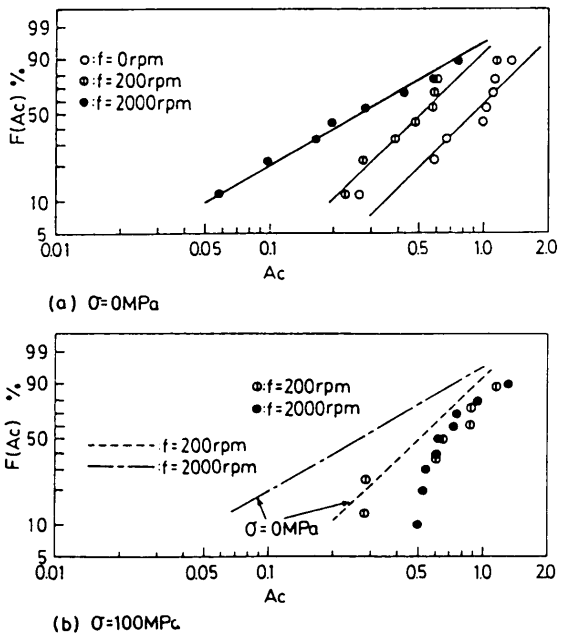

Fig. 5 The Weibull plots of A_c for both $\sigma=0$ MPa and 100 MPa

3.3 Shapes of corrosion pits

Figure 6 shows the variation in the aspect ratio, d_p/c, with $2c$, where $2c$ and d_p denote the pit length at the specimen surface and the pit depth, respectively. All the data obtained under conditions of $\sigma=0$ MPa, $\sigma=100$ MPa, $f=0$ rpm and $f=100$ rpm are plotted in this figure. As can be seen from this figure, there are slight differences between the data of $f=0$ rpm and $f=100$ rpm and also between the data of $\sigma=0$ MPa and $\sigma=100$ MPa. Hence, we can conclude that the shapes of the corrosion pits are independent of the fluid flow rate and stress amplitude. However, d_p/c shows the dependence on the pit length, $2c$. In the region $2c<100$ μm, the value of d_p/c is larger than 1, showing a pit shape deeper than a half sphere, while in the region $2c>100$ μm, the value of d_p/c decreases and approaches 1, indicating that the shape of the corrosion pit is a half sphere. The same results were also reported in a previous study[8].

4. Considerations

4.1 The effects of the fluid flow rate and stress amplitude on the pit initiation time

As a representative value of the pit initiation time shown in Fig. 4, we consider t_{ic50}, which denotes the value where the cumulative probability is 50%. Figure 7 shows the relationship between t_{ic50}, t_{ip50} and the fluid flow rate v plotted on the log- log diagram. In order to plot the pit initiation time at $v=0$, the horizontal

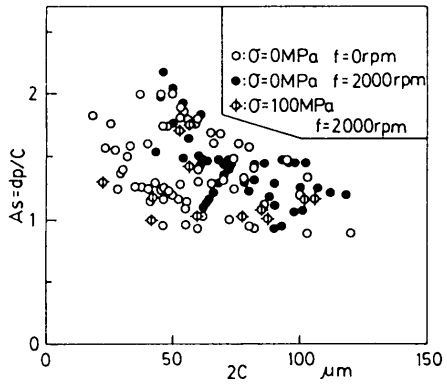

Fig. 6 Relationship between pit aspect ratio, d_p/c and pit length, $2c$

axis is taken as $(v+1)$. Asterisks (*) correspond to the data of t_{ip50}. As negligible differences between t_{ic50} and t_{ip50} are observed, we refer to both of them as t_{i50}, without distinction. From Fig. 7, we can see that there is a negative linear relationship between t_{i50} and $(v+1)$. Therefore, the following equation holds:

$$t_{i50}=B(v+1)^{-c}. \quad (2)$$

B and c are constants and their values are shown in this figure.

Oxygen diffusion-type corrosion and hydrogen evolution type corrosion are two corrosive reactions which occur in a solution. In neutral salt water, it is known that oxygen diffusion type corrosion occurs. As the reason why the fluid flow rate influences corrosive reactions, the following speculation can be considered. There may be a thin layer which adheres to the rotating specimen's surface. The thickness of this layer decreases with an increase in the fluid flow rate, thus promoting the diffusion of oxygen through this thin layer. Because the amount of oxygen at the specimen surface increases due to the above-mentioned diffusion, oxygen diffusion-type corrosion at the specimen surface is activated and hastens pit initiation.

Masuda et al.[8] performed corrosion fatigue tests in 3% sodium chloride aqueous solution using SUS 403, and reported that the pit initiation time in a test at 30 Hz is shorter than those at 0.03~3 Hz. Their result agrees with the present result.

Next, we compare the results of the loading test with those of the nonloading test. The pit initiation time in the test at $\sigma=100$ MPa is 1/7~1/10 shorter than that in the test at $\sigma=0$ MPa. Local plastic deformations occur on the specimen surface when cyclic stress is applied to the specimen. It is well known that a corrosive reaction occurs preferentially in these slipped regions. Accordingly, in the loading tests, the pit initiation time becomes shorter than that in the nonloading tests due to these active corrosive reactions.

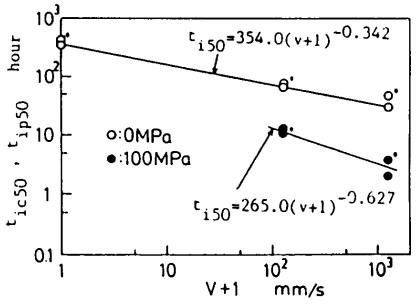

Fig. 7 Relationship between the pit initiation time and the fluid flow rate

4.2 Effects of the fluid flow rate and stress amplitude on the constant, A_c

The values of A_c, which denote conditions at a cumulative probability of 50% in Eq.(1), decrease with an increase in the fluid flow rate. These values are 0.9, 0.5 and 0.27 for $f=0$ rpm, $f=200$ rpm and $f=2\,000$ rpm, respectively.

In Kondo's experiment[9], the value of A_c was 0.33. Masuda et al.[8] reported that A_c reached a value of 0.63; on the other hand, Hinoshima et al. reported that A_c reached a value of 0.37. As shown above, the values of A_c differ from each other depending on the experimental conditions.

Kondo[9] explained theoretically why the value of A_c was 0.33, under the assumptions that both the corrosive current density and the pit density are constant and the shape of the corrosion pit is a half space. Engell, in Szklarska[11], reported that $A_c=1.3$ can be obtained under the following conditions: (a) Corrosive current density changes with time under a constant potential. (b) The number of corrosion pits increases with time. (c) The pit shape is a half space. (d) The current density within a corrosion pit is constant. In the present experiments, the number of corrosion pits increased with time in the experiment at $f=0$ rpm, while in the other experiments under the fluid flow rate, the number of corrosion pits was nearly constant throughout, except in the early stage of the process.

Considering the above experimental results and the proposed models[9],[11], the following speculation can be proposed. In an experiment with a stationary solution or a solution with a low flow rate, it is possible that the corrosive current changes with time because the number of corrosion pits increases with time. Thus, according to Engell's model[11], the value of A_c approaches 1. On the other hand, in a solution with a high fluid flow rate, the corrosive current is nearly constant, because the corrosion pits saturate in the early stage of the corrosion fatigue process and the number of pits assumes a constant value. Therefore, according to Kondo's model[9], A_c assumes a value near 0.33.

Next, we consider the change in A_c due to the application of stress. As shown in Fig. 5(b), the value of A_c in the loading test is larger than that in the nonloading test. For this reason, the corrosive current generated during the corrosion fatigue process is increased by the application of stress, because the number of initiation sites for the corrosive reaction in the specimen, such as slip steps and slip lines, increases as a result of the application of stress. The validity of the above speculation is supported by Endo and Komai's experimental results[12].

4.3 Effect of the fluid flow rate and stress amplitude on the pit growth rate

By differentiating Eq.(1) with time, the pit growth rate is given by the following equation:

$$d(2c)/dt=(2c)_0\cdot A_c\cdot t^{(A_c-1)}/t_{ic}^{A_c}$$
$$d(d_p)/dt=d_0\cdot A_p\cdot t^{(A_p-1)}/t_{ip}^{A_p} \quad (3)$$

Using Eq.(3), we investigated the distribution of the pit growth rates for two pit sizes, namely, 30 μm and 80 μm. The results are shown in Fig. 8. Taking the value at the cumulative probability of 50% as a representative value of the pit growth rate, the relationships between the representative pit growth rate and the fluid flow rate v are shown in Fig. 9. The horizontal axis denotes $(v+10)$. In the results of $\sigma=0$ MPa, shown in Fig. 9(a), the pit growth rate at the pit size of 30 μm increases with an increase in the fluid flow rate, showing marked fluid flow rate dependence, while at the pit size of 80 μm, the pit growth rate shows a smaller dependence on the fluid flow rate than that at the pit size of 30 μm. The pit growth rates at the pit size of 80 μm are smaller than those at the pit size of 30 μm, indicating that the pit growth rate decreases with an increase in pit size.

As shown above, the pit growth rates are dependent on the pit size. This result corresponds to the fact that, when the constant A_c or A_p in Eq.(1) is smaller than 1, the pit growth rates accelerate at the smaller pit size and decelerate at the larger pit size.

Comparing the pit growth rate at the specimen surface with that at the bottom of the pit, we find that the two values are nearly equal at the pit size of 30 μm, while, at the pit size of 80 μm, the former is larger than the latter. This means that the pit shape becomes flat with an increase in the pit size, corresponding to the results shown in Fig. 6.

The experimental tendencies observed in the results at $\sigma=0$ MPa are also observed in the results at $\sigma=100$ MPa shown in Fig. 9(b), but the pit growth rates at $\sigma=100$ MPa are 5~10 times larger than those at $\sigma=0$ MPa. The same result is also suggested in another study[13].

Sato et al.[14] reported that the fluid flow rate greatly influences the growth behavior of small corrosion pits, but only slightly influences the growth behavior of the large pit whose size exceeds a certain critical value. For this reason, they noted that a pit larger than the critical size is reduced to a passive state due to the formation of surface film on the dissolving surface. Harb and Alkire[15] performed finite-element simulation for the corrosion pit growth behavior, using the assumption that the specimen surface was covered with a surface film, and produced the same results as those reported by Sato et al.'s investigation.

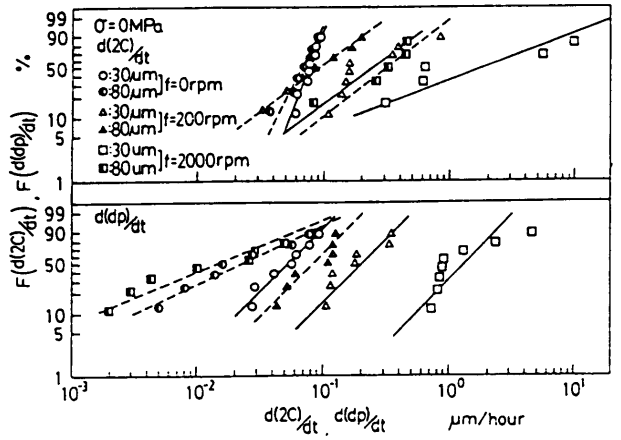

(a) $\sigma=0$ MPa

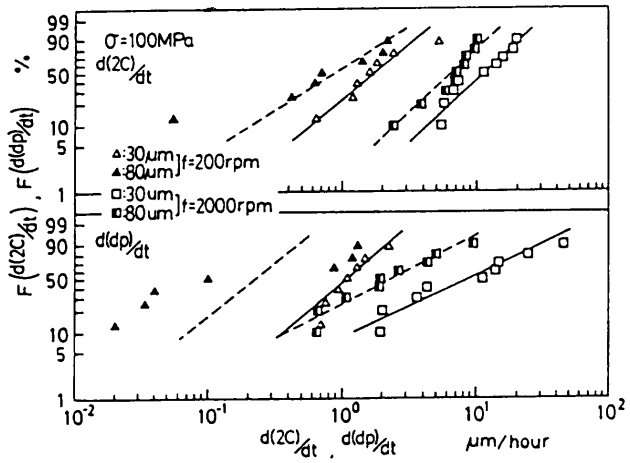

(b) $\sigma=100$ MPa

Fig. 8 Distribution of the pit growth rate

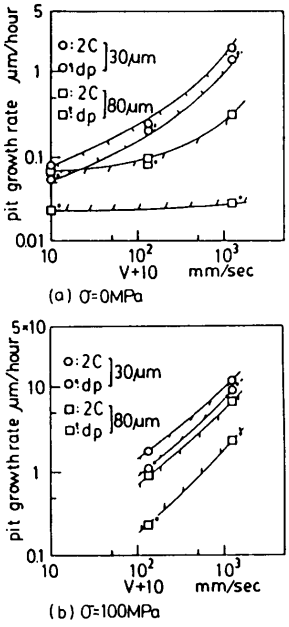

Fig. 9 Relationship between the representative pit growth rate and the fluid flow rate

From the above discussion, the influence of the fluid flow rate on the pit growth rate in nonloading tests is considered to be caused by the following process: In the early stage of pit growth, the bulk solution outside of the corrosion pit can easily enter the inside of the pit with an increase in the fluid flow rate, promote a corrosive reaction and accelerate the pit growth rate through the diffusion of oxygen in solution. However, thereafter, the formation of surface film on the specimen surface begins to occur with an increase in the pit size, lessening the effect of the fluid flow rate on the pit growth rate. The formation of the surface film occurs more easily within the corrosion pit than on the specimen surface. Accordingly, the pit growth rate in the direction of the pit depth becomes smaller than that in the direction of the specimen surface.

In loading tests, the pit growth rate increases with an increase in stress amplitude, because mechanochemical anodic dissolution is added to the above ordinary corrosion and, furthermore, the surface film is broken by the application of stress.

5. Conclusions

The initiation and growth behavior of corrosion pits were investigated using an annealed carbon steel, and the following results were obtained.

(1) The pit growth rate is given by Eq.(1) regardless of stress amplitude and the fluid flow rate.

(2) The pit initiation time decreases with an increase in the fluid flow rate, and the relationship between them is represented by Eq.(2). In the case where $\sigma=100$ MPa, the pit initiation time is shorter than that in the case where $\sigma=0$ MPa. The constant A_c in Eq.(1) decreases with an increase in the fluid flow rate, and increases with an increase in stress amplitude.

(3) The aspect ratio (d_p/c, d_p: pit depth, c: half-length of pit) is not affected by stress amplitude or the fluid flow rate. In the region of $2c<100$ μm, the aspect ratio has a value above 1.0, while in the region of $2c>100$ μm, the value of the aspect ratio is nearly 1.0, indicating a shape similar to a half sphere.

(4) In the nonloading test for a small pit size of 30 μm, the pit growth rate increases with an increase in the fluid flow rate, while in the region of a larger pit size of 80 μm, the pit growth rate shows a smaller effect of the fluid flow rate than at 30 μm, and shows a tendency to decrease with an increase in the pit size. In the case where $\sigma=100$ MPa, the pit growth rate is 5~10 times larger than that in the case where $\sigma=0$ MPa.

(5) The reasons why the fluid flow rate and stress amplitude affect the initiation and growth behavior of the corrosion pits can be summarized as the following three points: (i) The transport process of the chemical species from the bulk solution to the local pit, which is corroded, (ii) an anodic corrosive reaction including a mechanochemical reaction occurs here, and (iii) the formation of the surface film varies with pit size and location.

References

(1) Ishihara, S., Shiozawa, K. and Miyao, K., Distribution of Corrosion Fatigue Crack Length in Aluminum Alloy Prestrained by Pulling, J. Soc. Materials Science, Japan, (in Japanese), Vol. 31, No. 343(1982), p. 390.

(2) Ishihara, S., Maekawa, I., Shiozawa, K. and Miyao, K., Corrosion Fatigue Strength and Crack Growth in 0.16%C Carbon Steel Prestrained by Pulling, J. Soc. Materials Science, Japan, (in Japanese), Vol. 32, No. 363(1982), p. 1390.

(3) Tokaji, K., Ando, Z. and Mizutani, H., On Statistical Property of Fatigue Crack Length of High-Strength Steel, J. Soc. Materials Science, Japan, (in Japanese), Vol. 31, No. 343(1982), p. 1204.

(4) Tokaji, K., Ando, Z. and Hizutani, H., Small Fatigue Crack Initiation and Growth Behavior of High-Strength Low-Alloy Steel in Various Environments, J. Soc. Materials Science, Japan, (in Japanese), Vol. 33, No. 366(1984), p. 331.

(5) Kitagawa, H. and Nakasone, Y., A Monte Carlo Analysis Model of a Corrosion Fatigue Process Characterized by Initiation, Growth and Coalescence of Distributed Small Cracks, J. Soc. Materials Science, Japan, (in Japanese), Vol. 33, No. 364(1984), p. 14.

(6) Kawai, S. and Kasai, K., Considerations on the Allowable Stress in Corrosion Fatigue, Trans. Jpn. Soc. Mech. Eng.,(in Japanese), Vol. 51, No. 461, A(1985), p. 23.

(7) Komai, K., Minoshima, K. and Kim, G., Corrosion Fatigue Crack Initiation Behavior in 80 kgf/mm² High-Tensile Strength Steel Weldment in Synthetic Sea Water, J. Soc. Materials Science, Japan, (in Japanese), Vol. 36, No. 401(1987), p. 141.

(8) Masuda, C., Hirukawa, H., Abe, T. snd Nishijima, S., Corrosion Fatigue Life Prediction for SUS 403 Stainless Steel in 3%NaCl Aqueous Solution, Trans. Jpn. Soc. Mech. Eng.,(in Japanese), Vol. 52, No. 480, A(1986), p. 1764.

(9) Kondo, Y., Prediction Method of Corrosion Fatigue Crack Initiation Life Based on Corrosion Pit Growth Mechanism, Trans. Jpn. Soc. Mech. Eng.,(in Japanese), Vol. 53, No. 495, A(1987), p. 1983.

(10) Minoshima, K., Kiuchi, T. and Komai, K., Mechanical Conditions Dominating Cyclic Stress Corrosion Cracks of High-Strength Steel under Combined Cyclic/Static Multiaxial Loads, Trans. Jpn. Soc. Mech. Eng.,(in Japanese), Vol. 55, No.

519, A(1989), p. 2277.
(11) Szklarska, Z., Review of Literature on Pitting Corrosion Published Since 1960, Corrosion, Vol. 27, No. 6(1971), p. 223.
(12) Endo, K. and Komai, K., Electrochemical Observations on Corrosion Fatigue of Steel in Acid, J. Soc. Materials Science, Japan, (in Japanese), Vol. 17, No. 172(1968), p. 40.
(13) Noguchi, H., Nisitani, H. and Ogawa, T., Corrosion Fatigue Process of Annealed 0.50% Carbon Steel under Rotating Bending, Trans. Jpn. Soc. Mech. Eng., (in Japanese), Vol. 55, No. 511, A (1989), p. 386.
(14) Sato, N., Nakagawa, T., Kudo, K. and Sakashita, H., in Localized Corrosion (Staehle, R. W., Brown, B. F., Kruger, J, Agrawal, A. eds) NACE -3, Houston, (1974), p. 447.
(15) Harb, J. N. and Alkire, R. C., The Effect of Fluid Flow on Growth of Single Corrosion Pits, Corrosion Science, Vol. 29, No. 1(1989), p. 31.